Sensors and Actuators A 214 (2014) 111–119

Contents lists available at ScienceDirect

Sensors and Actuators A: Physical

journal homepage: www.elsevier.com/locate/sna

Hydrothermal synthesis of lead zirconate titanate (PZT or $Pb(Zr_{0.52}Ti_{0.48})O_3$) nano-particles using controlled ramping and cooling rates

Hsien-Lin Huang [a], G.Z. Cao [b], I.Y. Shen [a,*]

[a] Department of Mechanical Engineering, University of Washington, Seattle, WA 98195-2600, USA
[b] Department of Material Science & Engineering, University of Washington, Seattle, WA 98195-2120, USA

ARTICLE INFO

Article history:
Received 25 March 2013
Received in revised form 20 February 2014
Accepted 11 April 2014
Available online 21 April 2014

Keywords:
PZT
Lead-zirconate-titanate
Nanoparticles
Hydrothermal synthesis
Ramping and cooling rates
Excess lead

ABSTRACT

Lead zirconate titanate (PZT) nanoparticles with chemical composition $Pb(Zr_{0.52}Ti_{0.48})O_3$ hold many promising current and future applications, such as PZT ink for 3-D printing or seeds for PZT thick films. One common method is hydrothermal growth, in which temperature, duration, or mineralizer concentrations are optimized to produce PZT nanoparticles with controlled size and distribution. In this paper, we present a modified hydrothermal process to fabricate PZT nanoparticles. The novelty is to employ a high ramping rate (e.g., 20 °C/min) as well as a fast cooling rate (e.g., 5 °C/min). The former generates abrupt supersaturation to promote burst nucleation of PZT nanoparticles, and the latter provides a controlled termination of crystal growth. As a result, PZT nanoparticles with a size distribution ranging from 200 nm to 800 nm are obtained with good morphology and crystallinity. The chemical composition and crystal structure of the PZT nanoparticles are confirmed through use of energy dispersive X-Ray spectroscopy (EDS) and X-ray diffractometry (XRD). A cubic morphology is also confirmed via SEM images. The hydrothermal process is further modified with excess lead (from 20 wt.% to 80 wt.%) to significantly reduce amorphous phase and agglomeration of the PZT nanoparticles. Finally, an expedited hydrothermal manufacturing process was developed to substantially reduce the fabrication time.

1. Introduction

Lead zirconate titanate (PZT or $Pb(Zr_{0.52}Ti_{0.48})O_3$) nanoparticles, granules, or powder hold many promising current and future applications. For example, PZT powder can be suspended in solvent to form PZT ink [1–5], which can be used for various applications, such as 3-D printing. PZT nanoparticles can also be suspended in PZT sol to serve as seeds to lower sintering temperature of sol-gel derived PZT films [3]. PZT in granular forms can be pressed and sintered into specific shapes, such as disks and benders [6]. PZT nanoparticles can be embedded in silica or silane matrix to form sensors and actuators [5,7,8].

To enable these applications, the first task is to secure a large quantity of high-quality PZT nanoparticles. The nanoparticles must have narrow size distribution. Moreover, the size of the nanoparticles should be relatively insensitive to fabrication parameters. The size of the particles must be large enough (e.g., >200 nm) to ensure good piezoelectric properties. On the other hand, the size of the nanoparticles cannot be too large (e.g., <1 μm); otherwise, they may precipitate in PZT ink fabrication or clog 3-D printer nozzles. The PZT nanoparticles should have accurate stoichiometric composition (Ti/Zr mol ratio of 0.48/0.52), uniform morphology, and proper nano-crystal structures to ensure good piezoelectric properties. Since a large quantity of PZT nanoparticles is needed, the fabrication process must be simple and easy to control in order to achieve a high production rate.

Currently, there are two approaches to make PZT nanoparticles. The first way is a top-down approach often used in the industry [6,9]. In this approach, a large amount of PZT aggregates is fabricated by calcination and then milled down to the desired size. There are several major problems. First, the cubic morphology of PZT is damaged during the milling process; see Fig. 1. Second, the size and morphology of PZT particles vary widely. Also, contaminates are often introduced during the milling process. Therefore, the top-down approach does not generate high-quality PZT particles with good piezoelectric performance [10].

The second method is a bottom-up approach that is still under active investigation by various researchers. In this approach, PZT particles are grown and prefabricated from sol via a hydrothermal process, for example [11–17]. Size and quality of PZT nanoparticles

* Corresponding author. Tel.: +1 206 543 5718; fax: +1 206 685 8047.
E-mail address: ishen@u.washington.edu (I.Y. Shen).

http://dx.doi.org/10.1016/j.sna.2014.04.018
0924-4247/

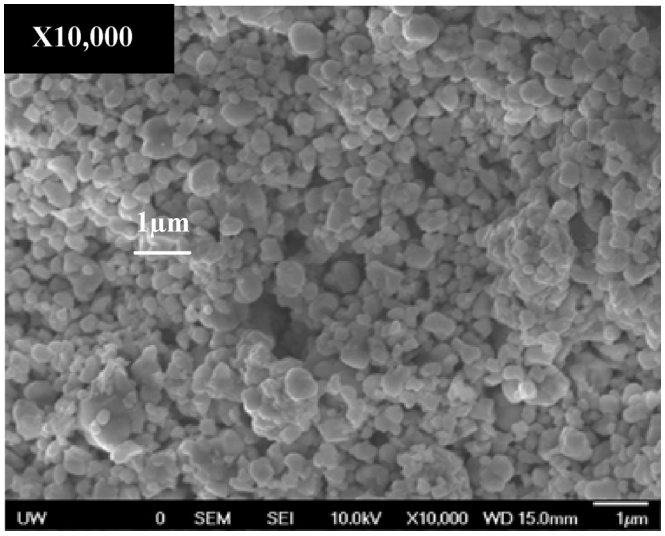

Fig. 1. SEM image of PZT particles from a top-down approach (×10,000).

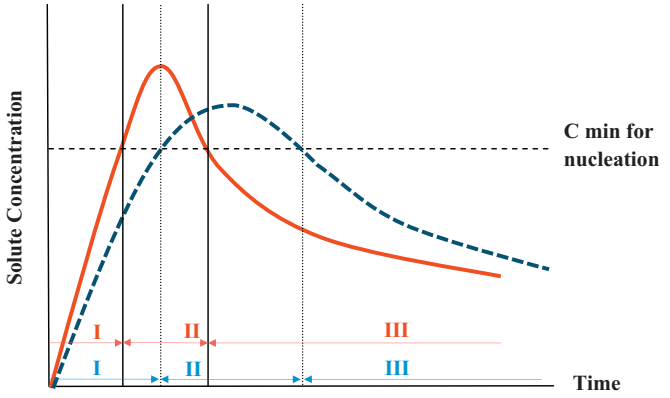

Fig. 2. Illustration of the process of nucleation and subsequent growth where region II is nucleation zone and region III is growth zone (dash line: lower ramping; solid line: higher ramping rate).

are controlled by various process parameters, such as temperature, time, and mineralizer concentration [11–15,17].

Although these hydrothermal processes have successfully resulted in functional PZT nanoparticles, they are not readily translational to real applications for several reasons. Some fabricated PZT particles do not have the desirable size (e.g., 5 μm for Harada and Dunn [14] and 25 nm for Das and Pramanil [16]). Other fabricated PZT nanoparticles heavily rely on mineralizer concentration to control the particle size. As a result, the particle size is very sensitive to mineralizer concentration and a uniform particle size becomes difficult to achieve [11,13,15]. In some cases, process time is as long as 24 h with long ramp-up and cool-off periods [13]. There is a strong need for a new hydrothermal process that is fast and easy to control the resulting particle size.

Motivated by these needs and applications, we present in this paper an effective way to produce PZT nanoparticles by controlling ramping and cooling rates of the hydrothermal process. The novelty of the paper is three-fold. First, we employ a high ramping rate to promote nucleation of PZT nanoparticles and follow up with a fast cooling rate to stop crystal growth. As a result, PZT nanoparticles with a precise size distribution ranging from 200 nm to 800 nm are obtained with good morphology and crystallinity. Second, we remove amorphous phase and reduce aggregation and agglomeration of PZT nanoparticles by adding extra lead in the hydrothermal process. Third, we develop an expedited hydrothermal process to reduce process time. In the expedited process, a furnace is maintained at the process temperature, whereas autoclaves containing PZT sol are placed in and out of the furnace to control the ramp-up and cooling rates. This setup eliminates an extremely time-consuming step of ramping up and cooling down the furnace, thus saving tremendous amount of process time making fabrication of a large amount of PZT nanoparticles possible.

Using the ramping and cooling rates to control size and distribution of PZT nanoparticles is also theoretically sound. Fig. 2 illustrates how solute concentration varies with respect to time during a hydrothermal process for high and low ramping and cooling rates [10]. In general, there are three regions in a hydrothermal process. Initially, there is no nucleation before the concentration reaches the minimum requirement saturation level (cf. Region I). Once nucleation starts, growth starts as well (cf. Region II). When the concentration falls below a critical concentration, nucleation stops but growth continues (cf. Region III).

By increasing the ramping rate, a super-saturation state is quickly achieved resulting in a very narrow region II; see the solid line in Fig. 2. Higher ramping rate means higher initial supersaturation and larger number of nucleation sites. This promotes formation of larger number yet smaller size of nuclei for a given solute concentration. Moreover, higher initial supersaturation means higher nucleation rate, as illustrated in Fig. 2. Therefore, nucleation will be dominated over growth in region II [10]. As a result, all nucleation would occur at the same time (high nucleation density) but with very limit time for growth, which subsequently leads to a smaller particle size and narrow size distribution.

By increasing the cooling rate, the concentration can be brought to a thermodynamic equilibrium very quickly to stop the crystal growth thus controlling the final particle size and morphology. Soon after the primary stage of the growth (region III in Fig. 2), Ostwald ripening occurs, leading to the secondary stage of nucleation and growth. In the secondary stage, aggregation process dominates leading to agglomeration and coagulation of the particles [18]. For hydrothermal processes, crystal growth highly depends on convective mass transfer of the dissolved part of the substance [19]. Increasing the cooling rate can significantly slow down the convective mass transfer and shorten the secondary stage, thus controlling the final particle size and improve the morphology effectively.

For the rest of the paper, we will first demonstrate how size and morphology of PZT nanoparticles can be controlled via ramping and cooling rates. We then demonstrate how excess lead in PZT feedstock improves morphology of the resulting PZT nanoparticles. Finally, an expedited hydrothermal process was developed and its process parameters are optimized for the chosen processing temperature of 200 °C.

2. PZT nano-particles via rate control

2.1. Feedstock preparation

The chemicals used to prepare the feedstock were tetra-iso-propylitanate (aka titanium isopropoxide, $Ti[OCH(CH_3)_2]_4$, denoted as TTIP), acetylacetone ($C_5H_8O_2$, denoted as AcAc), zirconium *n*-propoxide solution with 70% w/w in *n*-propanol ($Zr[O(CH_2)_2CH_3]_4$), and lead acetate trihydrate ($Pb(C_2H_3O_2)_2 \times 3H_2O$, denoted as $Pb(OAc)_2 \times 3H_2O$).

The feedstock preparation procedure was modified based on work of Su et al. [11]. TTIP was mixed with AcAc and the mixture was continuously stirred under room temperature for 4 h. $Zr[O(CH_2)_2CH_3]_4$ was then added into the mixture of TTIP and AcAc. The mixture was dropped into 1-M potassium hydroxide (KOH) solution. White zirconia-titania (theoretically $Zr_{0.52}Ti_{0.48}O$) precipitation was formed during this process. Centrifuge was used to separate out the precipitation. Then, the precipitation was washed

by centrifuge with DI water till the precipitation is pH neutral. The white gel was mixed with $Pb(OAc)_2 \times 3H_2O$ and added into *mineralizer* solution, which functions as a pH adjusting agent.

Mineralizer is very critical in the hydrothermal synthesis, because its concentration not only affects the particle size, morphology, and purity of the final product, but also controls processing time required to complete the synthesis [13,18,19]. In our study, potassium hydroxide (KOH) is chosen as the mineralizer solution. Since it is a very sensitive parameter, its concentration is adjusted to optimize the final product as the research progresses in stages (e.g., control of ramping and cooling rates, use of excess lead, and expedited hydrothermal process).

2.2. Hydrothermal synthesis

Hydrothermal synthesis of PZT suspension was carried out by *autogenous* pressure created in a 25-ml autoclave (Parr Pressure Vessel Model 4749). The autoclave was filled with 10 ml of PZT feedstock and the process temperature was set up to be 200 °C in a furnace (Barnstead Thermolyne Model 48000 Furnace). After the resulting PZT suspension was cooled down to room temperature, the suspension was centrifuged, washed with DI water till pH neutral, and then the PZT particles were oven-dried.

In the hydrothermal synthesis, combinations of various processing time and mineralizer concentration were tried because they could also affect the size and morphology of PZT nanoparticles. In general, processing time varied from 1 to 3 h, and mineralizer concentration from 2 M to 5 M.

Three ramping rates were used for the hydrothermal process: 5 °C/min, 10 °C/min, and 20 °C/min. In contrast, four cooling rates were used in this study: approximately 1.5 °C/min (very slow), 2.8 °C/min (medium), 3.6 °C/min (fast), and 5 °C/min (very fast). The cooling rate of 1.5 °C/min was achieved when the autoclave was cooled inside of the furnace with the door closed (i.e., with no air circulation). The cooling rate of 2.8 °C/min was achieved when the autoclave was cooled inside of the furnace with the door closed (i.e., with no air circulation) for 12 min and then with the door open (i.e., with natural air circulation) afterwards. The cooling rate of 3.6 °C/min was achieved when the autoclave was cooled inside of the furnace with the door closed (i.e., with no air circulation) for 5 min and with the door open (i.e., with natural air circulation) afterwards. The cooling rate of 5 °C/min was achieved when the autoclave was removed from the furnace immediately to cool under the room temperature. These cooling rates are approximate; they are estimated by measuring the temperature of the autoclave using a thermal couple over a period of time. For the rest of the paper, they will be referred as very slow (vs), medium (m), fast (f), and very fast (vf) cooling rates, respectively.

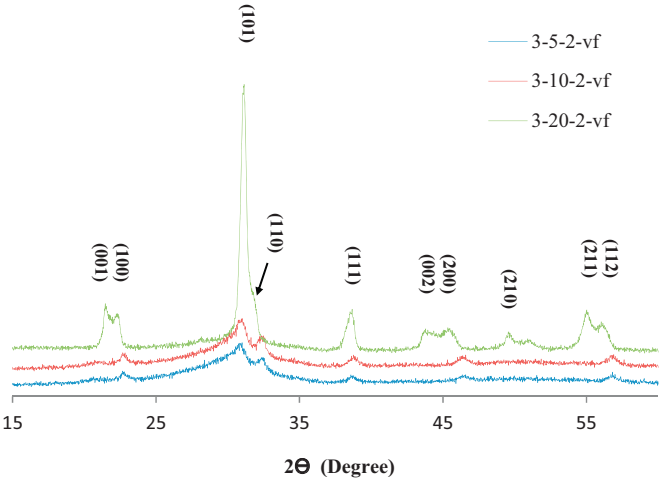

Fig. 3. XRD pattern of ramping trials for benchmark mineralizer concentration (2 M), processing time (3 h), and very fast cooling rate.

2.3. Effects of ramping rates

In studying the effects of ramping rates, we use a benchmark hydrothermal synthesis as follows: mineralizer concentration of 2 M, processing time of 3 h, and very fast cooling rate (5 °C/min). Moreover, test results are labeled using following notation A-B-C-D, where A is the processing time in hour, B is the ramping rate in

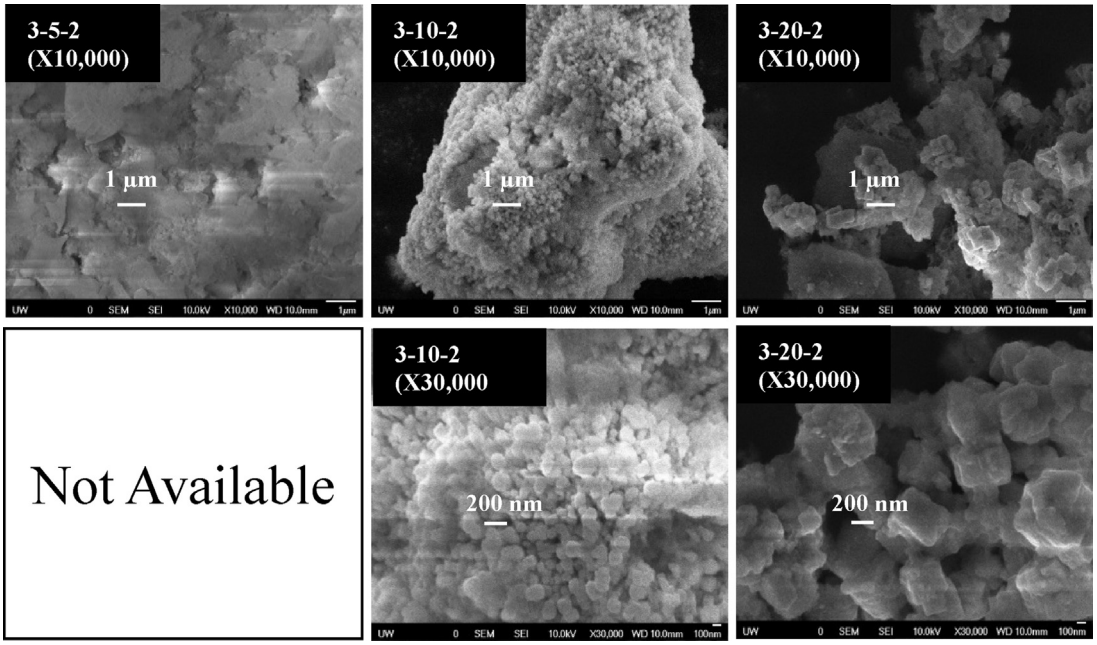

Fig. 4. SEM images of ramping trials for benchmark mineralizer concentration (2 M), processing time (3 h), and very fast cooling rate. Ramping rate: 5 °C/min (left), 10 °C/min (center) or 20 °C/min (right).

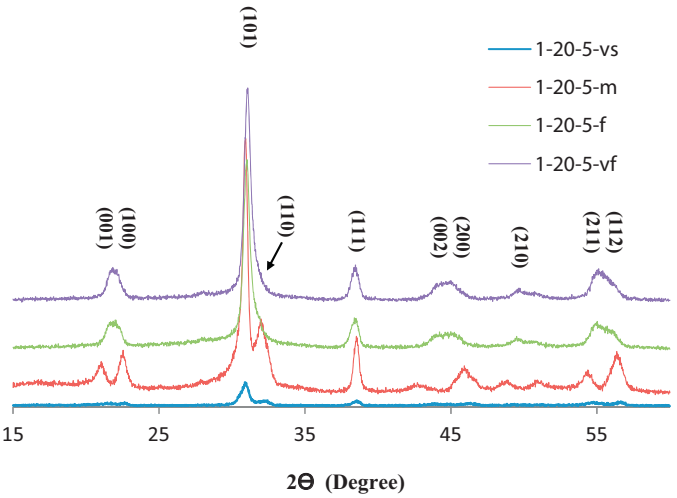

Fig. 5. XRD pattern of cooling trials for benchmark mineralizer concentration (5 M), processing time (1 h), and high ramping rate (20 °C/min).

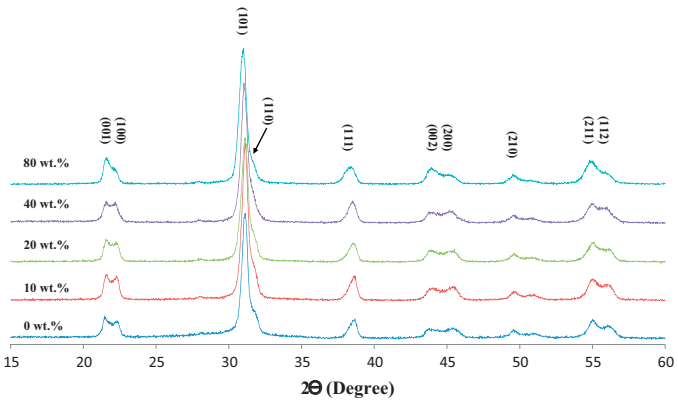

Fig. 7. XRD patterns for lead concentration trials with benchmark mineralizer concentration (2 M), processing time (3 h), ramping rate (20 °C/min), and cooling rate (very fast).

°C/min, C is the mineralizer concentration in M, and D is the cooling rate (e.g., "vf" for very fast cooling rate).

Fig. 3 shows X-ray diffractometry (XRD) measurements of PZT nanoparticles produced under the benchmark condition with three ramping rates. The XRD patterns are compared with a PZT database using JADE7.0 to confirm that the resulting product is indeed $Pb(Zr_{1-x}Ti_x)O_3$, and all major peaks are labeled in Fig. 3. Even though all XRD measurements show PZT composition and have the same peak locations (which means that overall similar crystal structure), the high ramping rate (20 °C/min) sample shows relatively small intensity in the secondary phases while the lower ramping rate samples (5 °C/min and 10 °C/min) contain readily secondary phase. For example, lower ramping rate samples (5 °C/min and 10 °C/min) contain obvious $PbTiO_3$ phase (around $2\theta \sim 32°$). At lower 2θ region, split peaks of (0 0 1) and (1 0 0) is observed indicating the presence of both rhombohedral ($PbZrO_3$) and tetragonal ($PbTiO_3$) phases [20]. These two peaks both have higher intensity than the database. It may be contributed by different composition of $Pb(Zr_x,Ti_{x-1})O_3$, such as $Pb(Zr_{0.8}Ti_{0.2})O_3$. All of them have board peaks at (0 0 2) and (2 0 0) which are contributed by $PbTiO_3$ formation. The broadened peak may be contributed by $PbZrO_3$ phase [14]. In addition, the intensity and sharpness of the XRD shown in the high ramping rate sample indicates increasing in crystallinity [13], which is an evidence of better PZT quality.

Fig. 4 also shows SEM images (magnification 10,000×) of the three samples with ramping rate 5 °C/min, 10 °C/min and 20 °C/min. The sample with the 5 °C/min ramping rate presents large aggregates and severe agglomeration. The sample with the 10 °C/min ramping rate shows large aggregates, and the sample with the 20 °C/min ramping rate has smaller aggregates. Although a higher ramping rate could reduce aggregation, it cannot completely eliminate the aggregation. Aggregation needs to be removed via other methods in order for these PZT nano-particles to be useful.

Fig. 4 also shows SEM images (magnification 30,000×) of PZT nano-particles produced under the two ramping rates: 10 °C/min and 20 °C/min. (The SEM 30,000× image for the sample with the 5 °C/min ramping rate could not be obtained due to the severe agglomeration.) As shown in Fig. 4, PZT sample produced under the ramping rate of 10 °C/min consists of very fine particles with size around 100 nm and their morphology is more spherical. In contrast, PZT produced under the ramping rate of 20 °C/min has particle size ranging from 200 nm to 600 nm. Also, morphology of the PZT nano-particles is clearly cubic. This indicates that the high ramping rate has a significant effect on the morphology.

The SEM images in Fig. 4 clearly proves that high ramping rate is favorable in achieving the desirable cubic morphology and particle size while reducing aggregation at the same time.

Controlling growth of PZT nano-particles via hydrothermal synthesis is indeed a fairly complex task because multiple process parameters are involved. In Fig. 4, we see a dramatic effect of the ramping rate given the benchmark parameters above. The effect of the ramping rate, however, may not be as dramatic under other process parameters (e.g., if a very slow cooling rate of 1.5 °C/min is used).

2.4. Effects of cooling rates

In studying the effects of cooling rates, we use a benchmark hydrothermal synthesis as follows: mineralizer concentration of 5 M, processing time of 1 h, and high ramping rate (20 °C/min). Four cooling rates are used as defined earlier. The same notation A-B-C-D is used to denote these four process parameters.

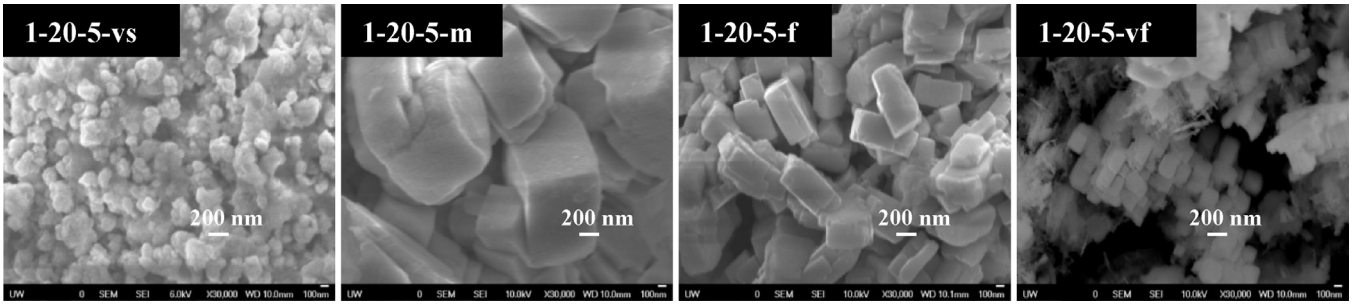

Fig. 6. SEM images of cooling trials for benchmark mineralizer concentration (5 M), processing time (1 h), and high ramping rate (20 °C/min). Cooling rate from left to right: very slow, medium, fast, and very fast.

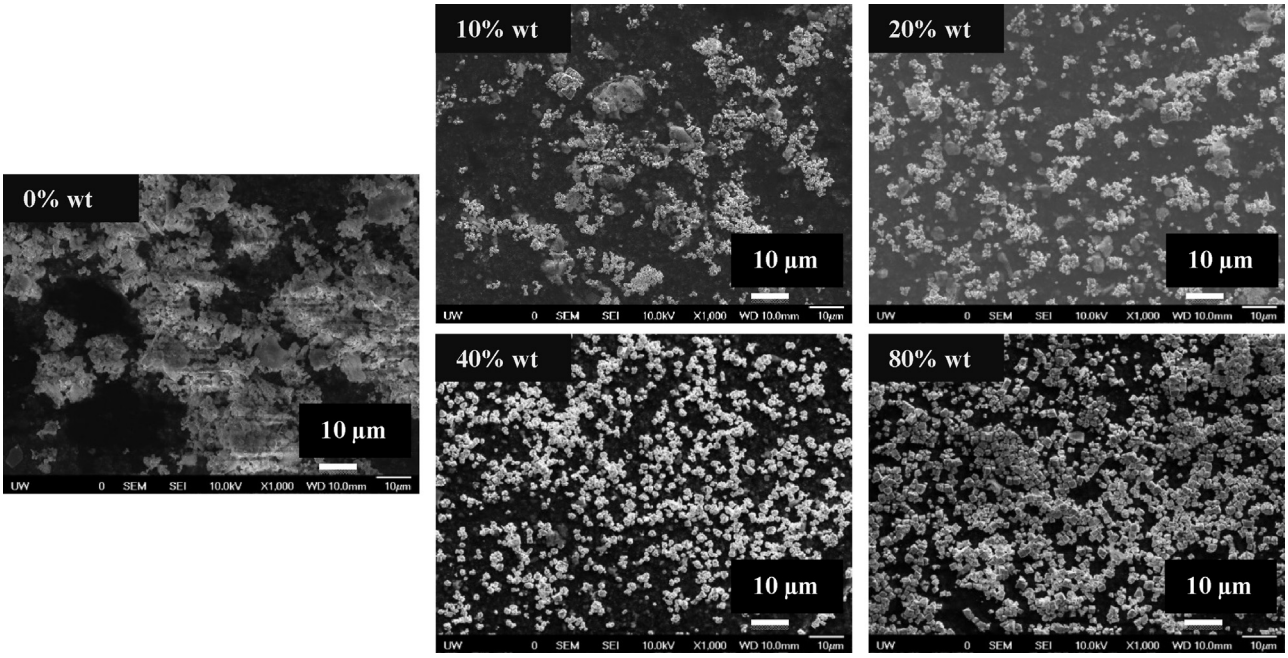

Fig. 8. SEM images on excess Pb samples (×1000) with benchmark mineralizer concentration (2 M), processing time (3 h), ramping rate (20 °C/min), and cooling rate (very fast).

Fig. 5 shows the XRD of the samples under the four cooling rates. From Fig. 5, peak locations do not change much with respect to the cooling rates. This implies that the cooling rates do not affect the chemical composition significantly. Nevertheless, secondary phases such as $PbTiO_3$ appear when the cooling rate is lower. For example, for the medium cooling rate (2.8 °C/min), secondary phases of $PbTiO_3$ are found (1 0 0) at the low-angle range, (1 1 0) and (0 0 2) at the mid-angle range, and (2 1 1) in the high-angle range. This shows that $PbTiO_3$ dominates when cooling rate is slow. This occurs because lower energy is needed in forming a tetragonal structure (e.g., $PbTiO_3$) [14]. Note that the sample with very slow cooling rate (1.5 °C/min) has poor crystallinity and result in lower peak intensity for all major peaks.

For the case of fast and very fast cooling rates, secondary phases are more difficult to identify because many peaks that correspond to the $PbTiO_3$ tetragonal phases overlap or merged with $PbZrO_3$ rhombohedral phases [14]. Nevertheless, the high intensity (1 1 0) peak of $PbTiO_3$ is not present, implying that there is no or low secondary phases.

Fig. 6 shows SEM images (magnification 30,000×) of the PZT nano-particles under the four cooling rates. The sample with very slow cooling rate (~1.5 °C/min) has severe agglomeration. Therefore, the particle size cannot be determined by the SEM image.

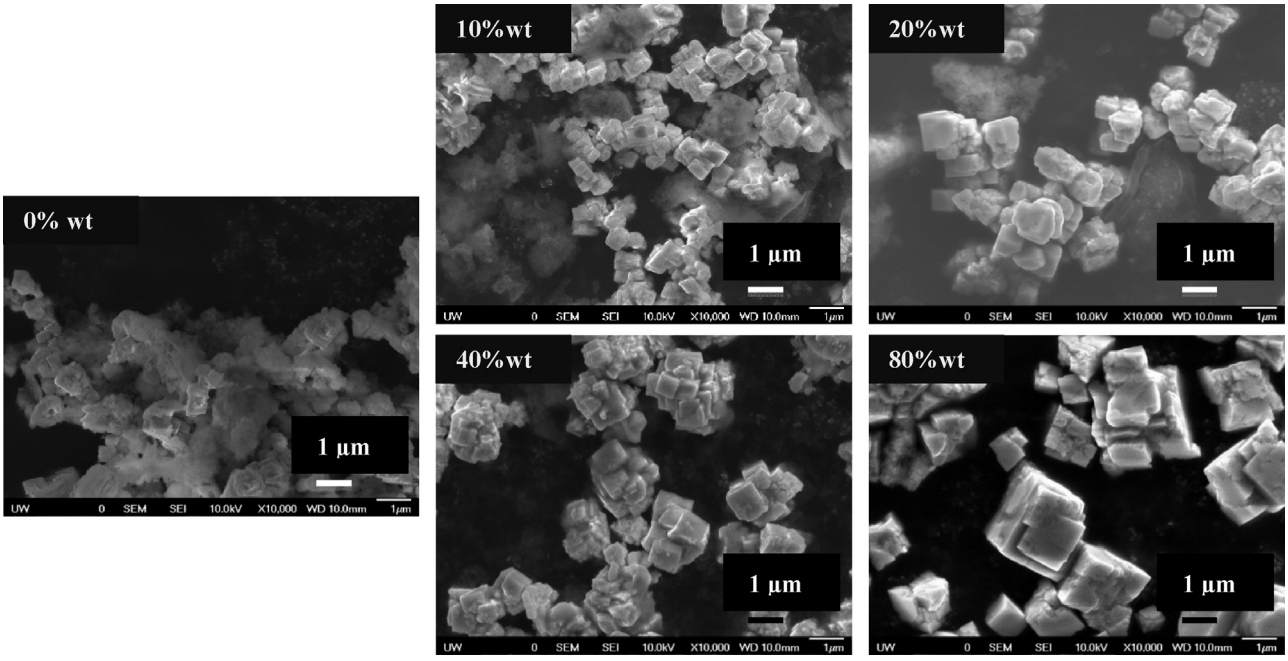

Fig. 9. SEM images for excess Pb (×10,000) with benchmark mineralizer concentration (2 M), processing time (3 h), ramping rate (20 °C/min), and cooling rate (very fast).

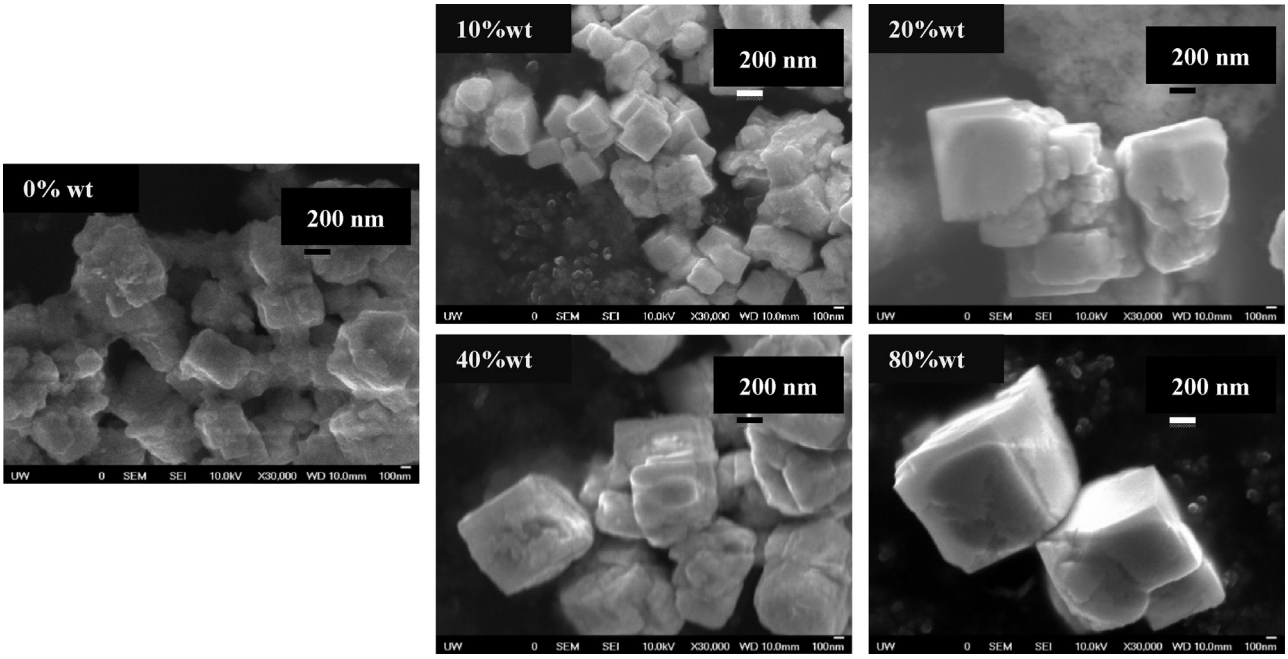

Fig. 10. SEM images for the excess Pb samples (×30,000) with benchmark mineralizer concentration (2 M), processing time (3 h), ramping rate (20 °C/min), and cooling rate (very fast).

Table 1
Effects of various lead concentrations.

Excess lead (wt.%)	Particle size (nm)	Aggregate size (μm)	Observation
0	N/A	>10	• Few particles around 1 μm • Large amount of aggregates
10	300 ± 100	1–10	• Few particles around 1 μm • Large amount of aggregates
20	400 ± 100	1–6	• Few particles around 1 μm
40	650 ± 200	1–2	• Most particles agglomerate into 1 μm size aggregates
80	800 ± 200	1–2	• Low degree of agglomeration

The sample with the medium cooling rate (~2.8 °C/min) results in high degree of agglomeration but the morphology is significantly improved as the cubic structure starts to appear. The medium cooling rate results in particle size in 600 nm to 800 nm range. The sample with the fast cooling rate (~3.6 °C/min) has particle size from 200 nm to 600 nm. Some samples show aggregates that are chemically bonded thus increasing overall particle size. As the cooling rate increases further, the overall particle size decreases to a range of 200 nm to 400 nm for very fast cooling rate (~5 °C/min).

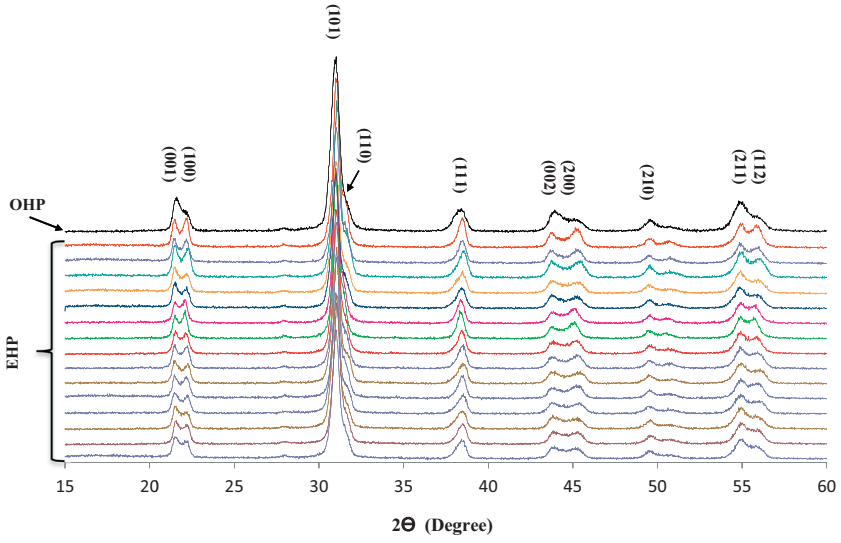

Fig. 11. Comparison of XRD patterns from OHP and EHP.

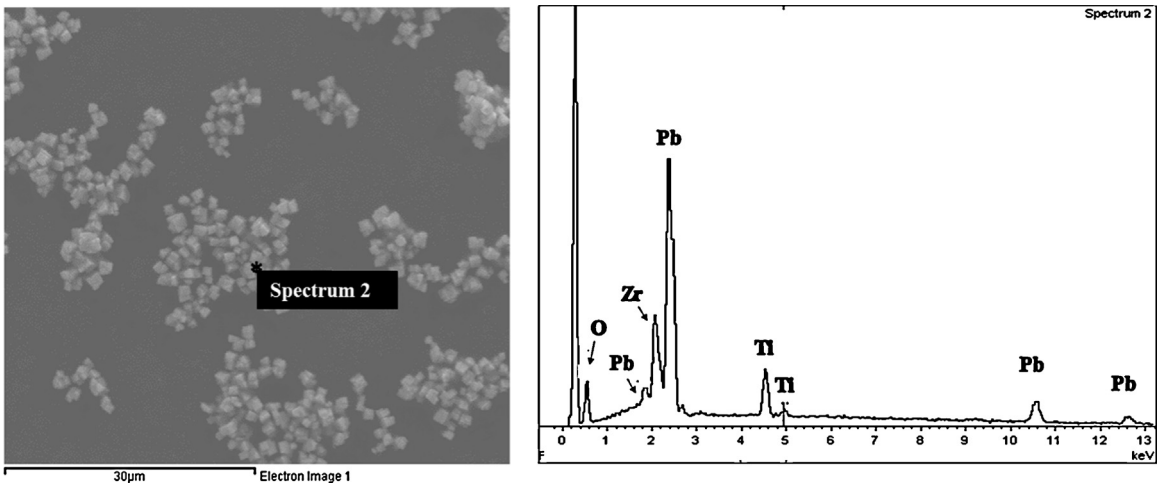

Fig. 12. Raw data of one EDS measurement as an example.

In conclusion, the SEM images in Fig. 6 shows that the cooling rate is an effective way to control the size of PZT nano-particles.

3. Removal of agglomeration and amorphous phase

Although we have successfully demonstrated that control of ramping and cooling rates is an effective way to control the size of PZT nano-particles in the range of 200 nm to 600 nm with a cubic crystal structure, there are two remaining problems. One is agglomeration and aggregation of the PZT nano-particles. The other is presence of amorphous phase in the PZT nano-particles. Use of excess lead could significantly alleviate both problems. It is very common that lead deficiency occurs in the beginning of the hydrothermal process. Therefore, supply of excess lead can effectively compensate the lead deficiency [15,17].

For example, Gersten [18] shows that agglomeration can be significantly reduced, if the mineralizer concentration (KOH) is between 2 M and 4 M and the lead concentration is between 0.5 M and 0.6 M. Traianidis et al. [15] uses excess lead to reduce amorphous phase. The lead deficiency causes the Pb/(Ti, Zr) molar ratio to fall below 1, which is required for PZT formation, thus lowering ion activities. Excess lead can ensure the required Pb/(Ti, Zr) molar ratio and high ion activities, resulting in improved crystallinity and reduced amorphous phase [15].

Based on Gersten's finding, we use the following benchmark parameters to study removal of the aggregation and amorphous state. The mineralizer concentration is 2 M, the processing time is 3 h, the ramping rate is 20 °C/min, and the cooling rate is very fast (~5 °C/min). Moreover, samples with 5 different lead concentrations are prepared: 0.38 M (0 wt.% lead excess), 0.41 M (10 wt.% lead excess), 0.45 M (20 wt.% lead excess), 0.53 M (40 wt.% lead excess), and 0.68 M (80 wt.% lead excess). The process temperature is 200 °C. For the samples that contained excess lead, the PZT precipitation was washed with DI water (as indicated earlier in Section 2.2) and 10 vol.% acetic acid to remove remaining unreacted lead source and other lead byproducts. Then PZT particles were washed with DI water again to bring the pH back to neutral.

Table 2
Elemental molar ratio of PZT nanoparticles from EHP based on EDS measurements.

	O	Pb	Ti	Zr
1	3	1	0.4746	0.5170
2	3	1	0.4831	0.5169
3	3	1	0.4796	0.5204
Avg.	3	1	0.4797	0.5181

Fig. 7 shows XRD measurements from samples processed under the benchmark condition. Five samples with excess lead of 0 wt.%, 10 wt.%, 20 wt.%, 40 wt.%, and 80 wt.% are measured. The XRD patterns are very consistent, indicating that the presence of excess lead does not affect crystal structures (e.g., crystal shape and lattice parameters).

The SEM images, shown in Figs. 8–10, demonstrate improvement of agglomeration, amorphous phases, and morphology when extra lead is introduced into the system. Five SEM images are shown in each figure from samples with 0 wt.% to 80 wt.% of excess lead. Fig. 8 (magnification 1000×) focuses on overall characteristics of the samples. It shows removal of amorphous regions (white cloudy regions in SEM images) as the excess lead concentration increases. At the same time, size of aggregates is reduced from more than 10 μm (0 wt.%) to 1–2 μm (>40 wt.%). Moreover, the size of the aggregates is much more uniform and not clustered together as the excess lead concentration increases.

Fig. 9 (magnification 10,000×) reveals structural changes of the aggregates. As lead concentration increases, the structure changes from complicated, folded cubes to simpler and more isolated cubes, which agrees with Geresten's results [18]. The degree of agglomeration is inversely proportional to the amount of excess lead used. Also, the amorphous phase is completed removed when the extra lead is above 40 wt.%.

Fig. 10 (magnification of 30,000×) demonstrates the change in particle size. For the sample with no extra lead, the particle size is difficult to be determined due to severe agglomeration. When the excess lead is present, the particle size increases from 300 nm (10 wt.% sample) to 800 nm (80 wt.% sample). Note that PZT particles of the 80 wt.% sample are almost free of agglomeration. Even though particle size increases with extra lead in the system, it still remains in the sub-micron range. For practical applications, it is better to have larger particles with less agglomeration than otherwise. Table 1 summarizes the effects of lead concentration on the particle and aggregate sizes.

4. Expedited hydrothermal process

In summary, the recipe we have developed thus far uses 80 wt.% excess lead and 2 M of KOH mineralizer concentration. The hydrothermal process includes high ramping rate 20 °C/min, process temperature 200 °C, process time of 3 h, and very fast cooling rate (~5 °C/min). This recipe reduces the presence of amorphous phases and the degree of agglomeration while maintaining desirable cubic morphology and correct chemical composition. For the rest of the

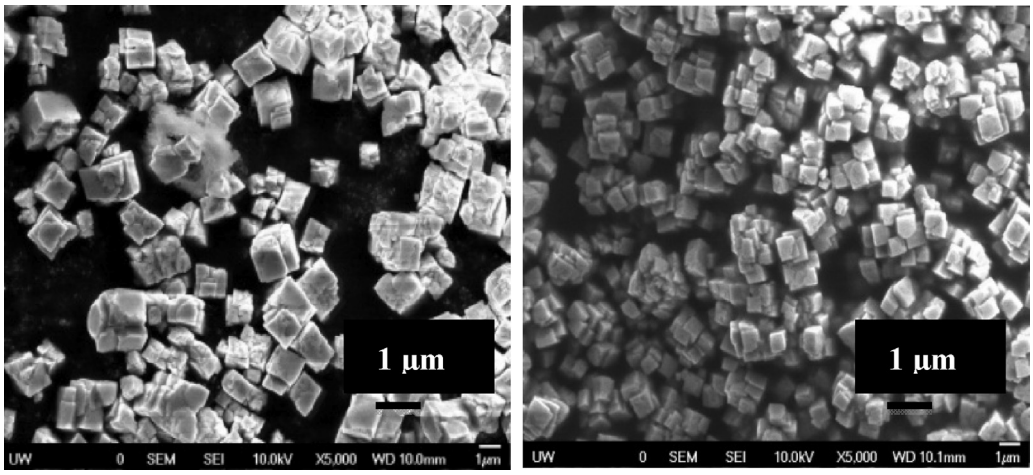

Fig. 13. SEM images (×5000) of OHP sample (left) and EHP sample (right).

paper, a process with these parameters is called the "optimal hydrothermal process" (OHP).

The OHP, however, has a major drawback—the overall time for the production of PZT nano-particles is very long. The bottleneck is the ramp-up of the furnace from the room temperature, because cooling of the furnace to the room temperature from a prior batch takes a long time (roughly 2 to 3 h). Also, 80 wt.% excess lead would increase manufacturing costs due to excess material and waste handling. Therefore, an expedited hydrothermal process is developed to reduce the overall process time while minimizing the excess lead contents. The detail procedure is described as follows.

First, no ramping is involved, and the furnace is maintained at 200 °C all the time. Second, the feedstock contains 2.5 M KOH mineralizer as well as 50 wt.% excess lead. Third, the autoclave with the feedstock is placed directly in the furnace and goes through hydrothermal growth for 2 h. Then the autoclave is removed from the furnace to cool down in the air under the room temperature. The process is repeated till the feedstock is used up. For the rest of the paper, this process is called the "expedited hydrothermal process" (EHP).

This process could potentially be used in a continuous manner in production lines. For example, a conveyor belt could continuously carry autoclaves into a furnace to perform hydrothermal growth. The duration of the hydrothermal growth inside the furnace could be controlled via the speed of the conveyor belt. Therefore, a large amount of nano-particles produced continuously with uniform properties.

Fig. 11 shows XRD patterns with the sample from OHP and EHP. The top black pattern is the sample with OHP (i.e., 80 wt.% excess lead) as a baseline, and the rest is from the samples with the EHP. There are several issues worth noting. First, peaks from all samples appear at the same location. This implies that all samples have similar chemical composition. Second, relative ratios of peak intensity are similar for all samples. This implies that crystal structures and crystallinity are similar for all samples. Note that peak intensity itself does not play a key role, because many other factors than

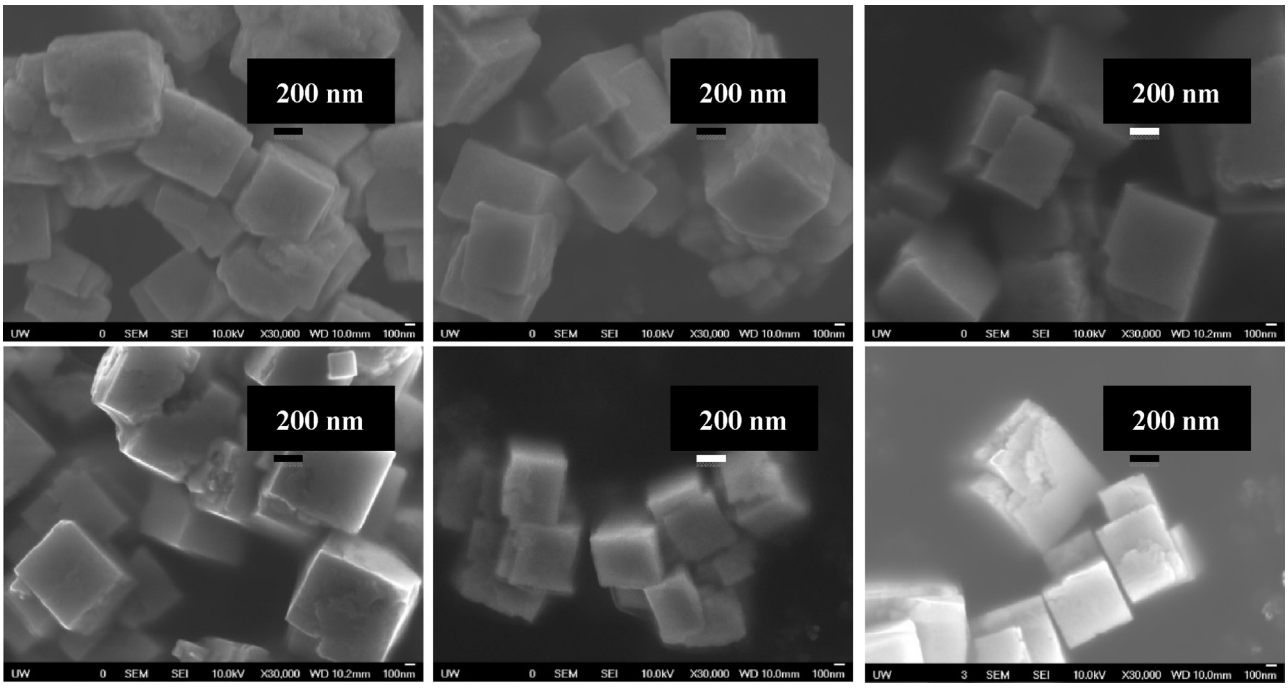

Fig. 14. SEM image (×30,000) of EHP samples from various batches.

crystal structures can affect the peak intensity. In contrast, relative intensity is a better way to identify variations among samples.

We have also confirmed the actual stoichiometric composition of the PZT nanoparticles using an energy dispersive spectrometer (EDS). Since XRD measurements show tiny sample variation, we thereby show EDS measurements of only one sample to save space. First of all, multiple particles are randomly picked from the sample for EDS measurements. Fig. 12 shows one measured spectrum as an example. The measured composition is then averaged. Table 2 shows the molar ratio of lead, titanium, and zirconium converted from the EDS measurements. Oxygen is balanced chemically. As the data shown, the overall chemical composition has the ratio of Zr/Ti = 0.52/0.48. Hence, PZT fabricated through EHP is indeed $Pb(Zr_{0.52}Ti_{0.48})O_3$.

Fig. 13 (magnification 5000×) compares the results from OHP and EHP samples. The aggregates in the EHP sample are slightly larger but all around 1 μm with little agglomeration. Also, the EHP sample shows no amorphous regions. These images demonstrate that ramping removal does not significantly affect the degree of agglomeration, aggregate size, and particle size. This is consistent with the observation that excess lead with greater than 40 wt.% will completely remove the amorphous state [18].

Fig. 14 (magnification 30,000×) shows EHP samples from various batches. Note that different batches may have some variations in mineralizer concentration due to difficulty in controlling precise weight of KOH (mineralizer) pellets. We estimate that the mineralizer concentration could at most vary between 2.5 M and 3.5 M from batch to batch. Nonetheless, all samples show low degree of agglomeration, 1–2 μm in aggregate size, and 300–600 nm in particle size. All the EHP samples do not contain amorphous regions and have good morphology. The EHP samples are quite uniform and are not sensitive to the change in mineralizer concentration. All evidence indicates that EHP is a very stable and reliable process.

5. Conclusions

The studies in this paper lead to the following conclusions.

(1) The size, distribution, and morphology of PZT nano-particles can be controlled effectively via ramping and cooling rates.
(2) A fast ramping rate results in sudden supersaturation and promotes nucleation with high density of nuclei. Consequently, small PZT nano-particles with narrow size distribution can be obtained.
(3) A fast cooling rate slows down crystal growth significantly. As a result, morphology of PZT nanoparticles is improved from large, non-uniform aggregates to small cubic particles with minor aggregation.
(4) Excess lead in feedstock reduces the degree of amorphous phases and agglomeration when the lead concentration is above 0.5 M.
(5) The best result occurs when the following process parameters are used: 80 wt.% excess lead, 2 M of KOH mineralizer concentration, fast ramping rate (20 °C/min), process temperature of 200 °C, process time of 3 h, and very fast cooling rate (~5 °C/min). The resulting PZT nano-particles present almost no amorphous phase or agglomeration, while maintaining desirable cubic morphology and correct chemical composition. The resulting particle size falls within 600 nm to 1000 nm.
(6) A simple expedited hydrothermal process is developed to boost the production rate without sacrificing the quality of PZT nanoparticles. The resulting PZT nanoparticles have a size between 300 nm to 600 nm, correct PZT composition, no amorphous phase, and a cubic crystal structure. Also, the quality of the resulting PZT nanoparticles is fairly consistent, as the mineralizer concentration varies within the window of 2.5 M to 3.5 M.

References

[1] Tianming Wang, Brian Derby, Ink-Jet Printing and Sintering of PZT, J. Am. Ceram. Soc. 88 (8) (2005) 2053–2058.
[2] K. Sivanandan, T. Asha, V. Achuthan, Kumar, Isaku Kanno, Fabrication and transverse piezoelectric characteristics of PZT thick-film actuators on alumina substrates, Sens. Actuators, A: Phys. 148 (2008) 134–137.
[3] Tomokazu Tanase, Yoshio Kobayashi, Mikio Konno, Preparation of lead zirconate titanate thin films with a combination of self-assembly and spin-coating techniques, Thin Solid Films 457 (2004) 264–269.
[4] Sung-Gap Lee, Effects of sol infiltration on the screen-printed lead zirconate titanate thick films, Mater. Lett. 61 (2007) 1982–1985.
[5] Chun-Hung Hsueh, Chia-Che Wu, Fabrication of lead zirconium titanium silica composite films on copper/polymide flexible substrates, Smart Mater. Struct. (19) (2010).
[6] PI Ceramic (Piezotechnology), Piezo Manufacturing Technology, <http://www.piceramic.com/piezo_technology.php>.
[7] Jeff Duce, Scott Johnston, I.Y. Shen, G.Z. Cao, Hsien-Lin Huang, Method and system of fabricating PZT nanoparticle ink based piezoelectric sensor, in: United States Patent No. 8,614,724, 2013.
[8] Sang Yup Kim, Toshio Tanimoto, Kenji Uchino, Chan Hee Nam, Sahn Nam, I.I. Woo Lee, Effects of PZT particle-enchanced ply interfaces on the vibration damping behavior of CFRP composites, Composites A: Appl. Sci. Manuf. 42 (2011) 1477–1482.
[9] Ronald Staut, Brain Julius, John Meiman, PZT Powder Manufacturing, 2010, <www.ceramicindustry.com>.
[10] G.Z. Cao, Y. Wang, Nanostructures and Nanomaterials: Synthesis, Properties, and Applications, Ch2-3, World Scientific Publishing Company, Singapore, 2011.
[11] B. Su, T.W. Button, C.B. Ponton, Control of the particle size and morphology of hydrothermally synthesized lead zirconate titanate powders, J. Mater. Sci. 39 (2004) 6439–6447.
[12] Yuan Deng, Li Liu, Yue Cheng, Ce-Wen Nan, Shu-jing Zhao, Hydrothermal synthesis and characterization of nanocrystalline PZT powders, Mater. Lett. 57 (2003) 1675–1678 (Elsevier Science).
[13] S.F. Wang, Y.R. Wang, T. Mahalingam, J.P. Chu, K.U. Lin, Characterization of hydrothermally synthesized lead zirconate titanate (PZT) ceramics, Mater. Chem. Phys. 87 (2004) 53–58.
[14] Scott Harada, Steve Dunn, Low temperature hydrothermal routes to various PZT stoichiometries, J. Electroceram. 20 (2008) 65–71 (Springer 2007).
[15] Maria Traianidis, Christian Courtois, Anne Leriche, Bernard Thierry, Hydrothermal synthesis of lead zirconium titanate (PZT) powders and their characteristics, J. Eur. Ceram. Soc. (19) (1999) 1023–1026.
[16] R.N. Das, P. Pramanil, In situ synthesis of nanosized PZT powders in the precursor material and the influence of pzrticle size on the dielectric property, Nanostruct. Mater. 10 (7) (1998) 1371–1377.
[17] Zhong-Cheng Qiu, Jia-Ping Zhou, Gangqiang Zhu, Peng Liu, Xiao-Bing Bian, Hydrothermal synthesis of $Pb(Zr_{0.52}Ti_{0.48})O_3$ powders at low temperature and low alkaline concentration, Bull. Mater. Sci. 32 (2) (2009) 193–197.
[18] B.L. Gersten, Crystal growth technology, in: K. Byrappa, T. Ohachi (Eds.), Growth of Muticoponent Perovskite Oxdie Crystals: Synthesis Conditions for the Hydrothermal Growth of Ferroelectric Powders, William Andrew Inc. Springer, New York, NY, 2001, pp. 300–333.
[19] K. Byrappa, Masahiro Yoshimura, Handbook of Hydrothermal Technology—A Technology for Crystal Growth and Materials Processing, Noyes Publications, New York, NY, 2001, pp. 164–184.
[20] Seung-Beom Cho, Magdalenda Oledzka, Richard E. Riman, Hydrothermal synthesis of acicular lead zirconate titanate (PZT), J. Cryst. Growth (226) (2001) 313–326.

Biographies

Hsien-Lin Huang is a Mechanical Engineering PhD student at the University of Washington and a Material and Processing engineer at the Boeing Company. Her graduate research is focused in the field of piezoelectric material and manufacturing processing. She graduated from the University of Washington in 2010 with a B.S. degree major in Material Science and Engineering and minor in Chemistry.

G.Z. Cao is Boeing-Steiner professor of Materials Science and Engineering, Professor of Chemical Engineering and Adjunct Professor of Mechanical Engineering at the University of Washington, Seattle, WA. He has published over 400 technical papers with 300 in archive journals and authored and edited 7 books. His current research focused on chemical processing of nanomaterials for solar cells, batteries, and supercapacitors as well as actuators and sensors.

I.Y. Shen received his B.S. and M.S. degrees from National Taiwan University and Ph.D. from the University of California (Berkeley), both in Mechanical Engineering. His general research area is vibration, sensing, and actuation. In particular, his expertise includes PZT thin-film micro-sensors/actuators and spindle/rotor dynamics. In the areas of PZT thin films, he is developing micro-sensors and actuators for future medical devices, such as hybrid cochlear implants. In the area of spindle and rotor dynamics, he is developing computational algorithms to predict vibration of complex rotating machines, such as hard disk drives and turbine engines.